HHS Public Access

Author manuscript

J Nucl Med. Author manuscript; available in PMC 2017 January 24.

Published in final edited form as:

J Nucl Med. 2016 June ; 57(6): 981–988. doi:10.2967/jnumed.115.167932.

Targeted Imaging of the Atypical Chemokine Receptor 3 (ACKR3/CXCR7) in Human Cancer Xenografts

Babak Behnam Azad[1], **Ala Lisok**[1], **Samit Chatterjee**[1], **John T. Poirier**[2], **Mrudula Pullambhatla**[1], **Gary D. Luker**[3], **Martin G. Pomper**[1,4], and **Sridhar Nimmagadda**[1,4]

[1]Department of Radiology and Radiological Science, Johns Hopkins University, Baltimore, MD, USA

[2]Department of Medicine, Memorial Sloan Kettering Cancer Center, New York, NY, USA

[3]Department of Radiology, University of Michigan, Ann Arbor, MI, USA

[4]Sidney Kimmel Comprehensive Cancer Center, Johns Hopkins University, Baltimore, MD, USA

Abstract

The atypical chemokine receptor ACKR3 (formerly CXCR7), overexpressed in various cancers compared to normal tissues, plays a pivotal role in adhesion, angiogenesis, tumorigenesis, metastasis and tumor cell survival. ACKR3 modulates the tumor microenvironment and regulates tumor growth. The therapeutic potential of ACKR3 has also been demonstrated in various murine models of human cancer. Literature findings underscore the importance of ACKR3 in disease progression and suggest it as an important diagnostic maker for non-invasive imaging of ACKR3 overexpressing malignancies. There are currently no reports on direct receptor-specific detection of ACKR3 expression. Here we report the evaluation of a radiolabeled ACKR3-targeted monoclonal antibody (ACKR3-mAb) for the non-invasive *in vivo* nuclear imaging of ACKR3 expression in human breast, lung and esophageal squamous cell carcinoma cancer xenografts.

Methods—ACKR3 transcripts were extracted from Cancer Cell Line Encyclopedia (CCLE), The Cancer Genome Atlas (TCGA) and the Clinical Lung Cancer Genome Project (CLCGP). ^{89}Zr-ACKR3-mAb was evaluated *in vitro* and subsequently *in vivo* by positron emission tomography (PET) and *ex vivo* biodistribution studies in mice xenografted with breast (MDA-MB-231-ACKR3 (231-AC-KR3), MDA-MB-231 (231), MCF7), lung (HCC95) or esophageal (KYSE520) cancer cells. In addition, ACKR3-mAb was radiolabeled with Iodine-125 and evaluated by single photon emission computed tomography (SPECT) imaging and *ex vivo* biodistribution studies.

Results—ACKR3 transcript levels were highest in lung squamous cell carcinoma (LUSC) among the 21 cancer type data extracted from TCGA. Also, CLCGP data showed that LUSC has the highest CXCR7 transcript levels compared to other lung cancer subtypes. The ^{89}Zr-ACKR3-mAb was produced in 80±5% radiochemical yields with >98% radiochemical purity. *In vitro* cell uptake of ^{89}Zr-ACKR3-mAb correlated with gradient levels of cell surface ACKR3 expression observed by flow cytometry. *In vivo* PET imaging and *ex vivo* biodistribution studies in mice with

Correspondence to: Sridhar Nimmagadda, Ph.D., Johns Hopkins Medical Institutions, 1550 Orleans Street, CRB II, Rm. 491, Baltimore, MD 21287, Phone: 410-502-6244, Fax: 410-614-3147, snimmag1@jhmi.edu.
First Author: Babak Behnam Azad, Ph.D., Johns Hopkins Medical Institutions, 1550 Orleans Street, CRB II, Rm. 470, Baltimore, MD 21287, Phone: 410-502-8171, Fax: 410-614-3147, bbehnam1@jhmi.edu, Status: Postdoctoral Fellow

breast, lung and esophageal cancer xenografts consistently showed enhanced ^{89}Zr-ACKR3-mAb uptake in high ACKR3 expressing tumors. SPECT imaging of ^{125}I-ACKR3-mAb showed the versatility of ACKR3-mAb for *in vivo* monitoring of ACKR3 expression.

Conclusions—Data from this study suggest ACKR3 to be a viable diagnostic marker and demonstrate the utility of radiolabeled ACKR3-mAb for *in vivo* visualization of ACKR3 overexpressing malignancies.

Keywords

Zirconium-89; Tumor microenvironment; Breast cancer; Lung cancer; Esophageal cancer; Molecular imaging

INTRODUCTION

The atypical chemokine receptor ACKR3, formerly CXCR7, is a 7-transmembrane G-protein coupled receptor, encoded by the RDC1 gene, with two endogenous ligands, CXCL11 and CXCL12. The ACKR3-CXCL11/12 interaction does not lead to typical G-protein coupled receptor -mediated calcium mobilization and chemotaxis, but rather the recruitment of β-arrestin, resulting in internalization of the receptor (1–5). For this reason, ACKR3 is referred to as an atypical chemokine receptor. ACKR3 expression, while low in healthy venule endothelium and arteriole smooth muscle cells, is upregulated with malignant transformation (6–12). ACKR3 modulates the tumor microenvironment by mediating adhesion, angiogenesis, tumorigenesis and tumor cell survival (2). It also oversees tumor growth by regulating angiogenic, proliferative and signaling pathways (13,14).

ACKR3 is overexpressed in >30% of all breast cancers (including in situ and invasive ductal and lobular carcinomas), with 97% of studied specimens (106 of 109) exhibiting robust vascular ACKR3 staining with undetectable expression in normal breast tissues (10,15). This overexpression is correlated with poor overall survival and lung metastasis-free survival in patients with invasive ductal carcinomas as well as reduced relapse-free survival in patients with ER+ breast cancer (14,16). ACKR3 overexpression has also been confirmed in 45% of esophageal squamous cell carcinomas (7) and 60% of LUSC with undetectable expression in adjacent normal lungs. In patients with lung cancer, this overexpression is correlated with advanced stage, lymphatic invasion and poor survival rates (17,18). Microarray profiling of LUSC in transgenic mouse models has also shown ACKR3 to be highest expressed (19). Similar results have been reported in other malignancies including soft tissue tumors, cervical, renal and prostate cancer where ACKR3 expression is 2–3 fold higher in prostate cancer and metastatic legions, compared to benign and prostatic intraepithelial neoplasia (8,10).

The functional role of ACKR3 in modulating the tumor microenvironment has become more apparent with recent reports suggesting ACKR3 as a therapeutic target for reducing tumor burden and angiogenesis (20). Attesting to this fact, small molecule ACKR3 inhibitors have been shown to limit tumor growth in syngenic mouse models of human breast cancer, B lymphoma and lung carcinoma mouse models (2). ACKR3 also regulates metastasis by acting as a critical scavenger of CXCL12, a key chemokine responsible for homing of

primary tumor cells to CXCL12-rich metastatic sites such as bone marrow, lungs and brain (21,22). In addition, the transforming growth factor-β1 (TGF-β1), a key regulator of the tumor microenvironment and chemokine gradients (23,24), increases ACKR3 expression in the lung tumor microenvironment (20). Perhaps more important is that ACKR3 silencing results in reversal of TGF-β1-induced changes on epithelial-mesenchymal transition, cancer cell invasion and migration. Patients with high ACKR3 and TGF-β1 levels, however, exhibited worse prognosis and survival rates. Taken together, these findings underscore the pathological importance of ACKR3 in cancer regulation and progression to metastasis. They also suggest the importance of ACKR3 as a valuable prognostic marker and urge the need for non-invasive detection and monitoring of ACKR3 expression.

There are currently no reports on the direct, receptor specific *in vivo* detection of ACKR3 expression. In one report, a fluorophore-tagged CXCL12 analogue was utilized for *in vivo* optical imaging of ACKR3 expression (25). However, while CXCL12 exhibits a high ACKR3 binding affinity, its relatively short half-life makes it a poor choice for further development as an imaging agent and routine clinical use (26). In addition, limited depth penetration associated with optical imaging could further limit the utility of that agent. More importantly, however, is the fact that CXCL12 binds to both CXCR4 and ACKR3 receptors. As a result, the observed signal could not be discretely assigned to ACKR3 expression alone, further conveying the need for ACKR3-specific imaging agents.

For a more comprehensive overview of ACKR3 expression in cell lines and tumors, we first extracted mRNA expression levels from CCLE, TCGA and CLCGP. We then tested the feasibility of *in vivo* imaging of ACKR3 expression by PET using a ^{89}Zr-labeled ACKR3-targeted monoclonal antibody (^{89}Zr-ACKR3-mAb). The specificity of the high affinity ACKR3 antibody clone used in our study (clone 11G8; IC50 = 8.1nM against ^{125}I-CXCL12 and 25nM against ^{125}I-CXCL11) has been illustrated in literature reports (1,6,10,27). This clone has also been shown to block CXCL11 and CXCL12 binding to CXCR7 and inhibit chemokine-mediated β-arrestin2 recruitment (1). The ability of ^{89}Zr-ACKR3-mAb to detect ACKR3 expression was demonstrated in NOG (NOD/Shi-*scid*/IL-2Rγ^{null}) mice xenografted with human breast, lung or esophageal cancers. These malignancies were selected as proof of concept for *in vivo* imaging of ACKR3 expression as they all overexpress this receptor at varying levels (7,10). In addition, the applicability of ACKR3-mAb for use with other modalities was also illustrated SPECT imaging of ^{125}I-labeled ACKR3-mAb (^{125}I-ACKR3-mAb) in mice bearing human breast cancer xenografts. Our results demonstrate the application of radiolabeled ACKR3-mAb for *in vivo* visualization of ACKR3 overexpressing cancers and suggest ACKR3 as a viable diagnostic marker.

MATERIALS AND METHODS

Please refer to the supplementary information for detailed methods and experimental procedures.

RESULTS

ACKR3 expression in various cancers by CCLE, TCGA and CLCGP

A comprehensive overview of ACKR3 expression in various tumor types has not yet been reported. Therefore, we first extracted mRNA data from CCLE (Fig. 1), which showed elevated ACKR3 mRNA expression levels in multiple malignancies, including upper aerodigestive tract, kidney and esophageal cancer cell lines. Multiple cell lines with high ACKR3 expression levels were also noted in breast and lung LUSC tumor types. To further explore the ACKR3 expression profile in human tumors, we extracted ACKR3 mRNA expression levels from TCGA (Fig. 1). Data from 21 human tumor types showed the highest ACKR3 mRNA expression in LUSC with esophageal and breast (BRCA) cancers centered in the expression profile. Similarly, CXCR7 expression levels were highest in LUSC among the lung cancer subtype data extracted from CLCGP (Fig. 1). As a result, we focused on beast, esophageal and LUSC tumor types for noninvasive detection of ACKR3 expression.

Generation of ^{89}Zr-ACKR3-mAb

Antibodies were first conjugated with desferrioxamine (on average 2 desferrioxamine molecules per antibody, Supplemental Fig. 1) via isothiocyanate-amine chemistry, for subsequent ^{89}Zr-chelation. Radiolabeling with Zr-89 was optimized with radiochemical yields of 85 ± 5% and radiochemical purities > 98% as determined by instant thin layer chromatography (Supplemental Fig. 2). Specific activities were 296±18 MBq/mg (8.0 ± 0.5 mCi/mg) for *in vitro* studies and 92±7 MBq/mg (2.5 ± 0.2 mCi/mg) for *in vivo* studies. The integrity of ACKR3-mAb at various levels of modification (desferrioxamine conjugation as well as radiolabeling) was confirmed using sodium dodecyl sulfate polyacrylamide gel electrophoresis (Coomassie staining), under reducing and non-reducing conditions, and autoradiography, respectively (Supplemental Fig. 3).

^{89}Zr-ACKR3-mAb exhibits rapid internalization *in vitro*

The immunoreactive fraction of the radiolabeled antibody, as determined by Lindmo assay (28), was 95±4% (Supplemental Fig. 4A). *In vitro* ^{89}Zr-ACKR3-mAb uptake in 231-ACKR3 cells, with 231 cells as the negative control, demonstrated rapid internalization over 2hrs of incubation, but plateaued between thereafter, up to 6hrs of incubation (Fig. 2C). ACKR3 internalization was significantly reduced at 4°C as evident by lower ^{89}Zr-ACKR3-mAb uptake.

In vitro ^{89}Zr-ACKR3-mAb uptake correlates with ACKR3 expression levels

To evaluate ^{89}Zr-ACKR3-mAb *in vitro*, uptake assays were carried out in breast, LUSC and esophageal squamous cell carcinoma cancer cell lines. ACKR3 Expression levels were evaluated by flow cytometry and were shown to be in the order of 231-ACKR3>MCF7>MDA-MB-231-CXCR4 (231-CXCR4)>KYSE520>HCC95>231 (Fig. 2A). Uptake of ^{89}Zr-ACKR3-mAb (Fig. 2B) correlated with ACKR3 expression levels detected by flow cytometry. This selective binding was inhibited with 10meq of unlabeled ACKR3-mAb in 231-ACKR3 and 231 cells, further confirming an ACKR3-mediated uptake. In addition, the selectivity of ^{89}Zr-ACKR3-mAb for ACKR3 over CXCR4, a structurally

similar receptor that forms heterodimers with ACKR3, was illustrated by an approximately 15 fold higher uptake in 231-ACKR3 cells (Fig. 2B). This finding was further confirmed with minimal uptake of ^{89}Zr-ACKR3-mAb by two additional cell lines exhibiting high CXCR4 and low CXCR4 expression levels (Supplemental Fig. 4B).

ImmunoPET demonstrates enhanced ^{89}Zr-ACKR3-mAbuptake by TNBC and ER+ luminal A breast cancer xenografts

The specific activity of ^{89}Zr-ACKR3-mAb for *in vivo* PET-CT imaging studies was optimized with *ex vivo* biodistribution studies in NOG mice xenografted with 231-ACKR3 and the parental 231 cells. The highest 231-ACKR3 to 231 tumor ratio (5.1±0.4) was observed with a 9MBq/100μg (250μCi/100μg) mAb dose per mouse (Fig. 2D), which was used thereafter for imaging studies.

PET-CT imaging of NOG mice baring 231-ACKR3 and 231 tumors over 120h indicated preferential uptake of ^{89}Zr-ACKR3-mAb by 231-ACKR3, compared to 231, tumors (Fig. 3A). These results were quantified by *ex vivo* biodistribution studies, showing the highest tumor uptake of 12.1±0.2%ID/g in 231-ACKR3 tumors 48hrs post injection (Fig. 3A). Non-specific retention was observed in liver, spleen and kidneys. *In vivo* specificity of ACKR3-mediated uptake was confirmed by blocking studies, showing a significant reduction in ^{89}Zr-ACKR3-mAb uptake by 231-ACKR3 tumors in PET-CT images (Fig. 3B). These results were further supported by *in vivo* image analysis, which revealed a 41% decrease in tumor uptake (25.2±1.4%ID/cc for non-blocked versus 14.9±1.5%ID/cc for blocked) with the blocking dose (Fig. 3B). Higher ACKR3 immunoreactivity in excised 231-ACKR3, compared to 231, tumors further supported ACKR3-mediated ^{89}Zr-ACKR3-mAb uptake (Fig. 3C).

Following the target specificity observed in subcutaneous TNBC xenografts, we tested the applicability of ^{89}Zr-ACKR3-mAb for non-invasive detection of ACKR3 expression in other breast tumor subtypes. ^{89}Zr-ACKR3-mAb-PET successfully visualized ACKR3 overexpressing ER+ luminal A MCF-7 breast cancer xenografts in NOG mice (Fig. 4). Quantitative analysis of PET images (Figure 4) revealed a 6.3±0.5%ID/cc uptake in MCF7 tumors 48hrs post injection.

^{89}Zr-ACKR3-mAb-PET for visualization of ACKR3 expression in other cancers

Similar results were obtained in HCC95 NOG mice. ImmunoPET (Fig. 4) with ^{89}Zr-ACKR3-mAb was able to detect ACKR3 expression in HCC95 tumors. Quantitative image analysis (Fig. 4) showed a 4.7±0.1%ID/cc uptake in HCC95 tumors, 48hrs post injection. In KYSE520/231 xenografts, ^{89}Zr-ACKR3-mAb was preferentially retained in high ACKR3 expressing KYSE520, compared to 231 control tumors (Fig. 5A). *Ex vivo* biodistribution in these xenografts showed 10.7±0.4%ID/g in KYSE520 and 5.9±0.2%ID/g in 231 tumors, 48hrs post injection (Fig. 5A). ImmunoPET imaging following *in vivo* blocking, as well the corresponding *in vivo* image analysis, demonstrated a significant reduction (11.46±3.47%ID/cc) in ^{89}Zr-ACKR3-mAb uptake by KYSE520 tumors (Fig. 5B), further confirming the specificity of ^{89}Zr-ACKR3-mAb for ACKR3 receptors. This ACKR3-

mediated uptake was also supported by enhanced ACKR3 immunoreactivity in excised KYSE520, compared to 231, tumors (Fig. 5C).

^{125}I-ACKR3-mAb-SPECT for non-invasive *in vivo* detection of ACKR3 expression

The feasibility of radiolabeled ACKR3-mAb for *in vivo* visualization of ACKR3 expression with other modalities was assessed by SPECT imaging of ^{125}I-ACKR3-mAb. While ^{125}I-ACKR3-mAb was initially non-specifically taken up by 231 tumors, preferential uptake and retention by 231-ACKR3 tumors was observed 120hrs post injection (Fig. 6). Non-specific retention of ^{125}I-ACKR3-mAb was observed in the thyroid (owing to *in vivo* de-iodination), liver, spleen, lungs, small intestines and kidneys. *Ex vivo* biodistribution studies with ^{125}I-ACKR3-mAb, 120hrs p.i., in the same mouse xenografts showed a ^{125}I-ACKR3-mAb uptake of 4.3±0.3%ID/g in 231-ACKR3 and 1.6±0.6%ID/g in 231 tumors (Fig. 6). These findings confirm the applicability of radiolabeled ACKR3-mAb for *in vivo* visualization of ACKR3 overexpressing tumors using either PET or SPECT modalities.

DISCUSSION

Upregulation of ACKR3 expression occurs with malignant transformation. This overexpression is observed in an array of malignancies including soft tissues tumors, breast, lung, esophageal, and prostate cancers (7,8,10). Recent accumulating literature has established the pivotal role of ACKR3 in modulating the tumor microenvironment and regulating tumor cell adhesion, angiogenesis, tumorigenesis and metastasis (13,14). The critical role of ACKR3 in cell migration and disease progression has also been further implicated through its scavenging of CXCL12 and heterodimerziation with CXCR4, both of which are key variables in cell migration during developmental, immune response and pathological processes (21,22,29,30). Although accumulating literature reports have emphasized the pathological significance of ACKR3 expression, there are currently no reports on direct receptor-specific imaging of ACKR3. In this report, we assessed ^{89}Zr-ACKR3-mAb-PET for the non-invasive *in vivo* detection of ACKR3 overexpression.

In vitro evaluation of ^{89}Zr-ACKR3-mAb in human breast, lung and esophageal squamous cell carcinoma cell lines showed an uptake correlating with cell-surface ACKR3 expression and demonstrated the suitability of this mAb for *in vivo* evaluation. In addition, in agreement with the ACKR3 specificity shown for the 11G8 clone (1,6,10,27), our *in vitro* data also support preferential selectivity of ^{89}Zr-ACKR3-mAb for ACKR3 over CXCR4. However, given the reported constitutive formation of ACKR3-CXCR4 dimers, visualization of ^{89}Zr-ACKR3-mAb uptake may reflect monomeric or homo/hetero-dimeric ACKR3. *In vivo* ^{89}Zr-ACKR3-mAb-PET and *ex vivo* biodistribution studies in mice harboring TNBC tumors with graded ACKR3 expression levels agreed with *in vitro* findings, showing a direct correlation between ^{89}Zr-ACKR3-mAb uptake and ACKR3 expression. This ACKR3-mediated uptake was confirmed by *in vivo* blocking, which resulted in a significant reduction of signal in high ACKR3-expressing tumors as indicated by PET-CT and quantitative *in vivo* image analysis. ^{89}Zr-ACKR3-mAb-PET was also able to visualize ACKR3 expression in other tumor models including MCF7 ER+ luminal A breast cancer, lung and esophageal squamous cell carcinoma xenografts. In addition, our results also show the capability of radiolabeled

ACKR3-mAb for *in vivo* ACKR3 imaging by other nuclear modalities. This was demonstrated by ^{125}I-ACKR3-mAb-SPECT in mice xenografted with TNBC, thereby proving the flexibility of this approach for a broader range of imaging applications. It is important to note that because the ACKR3 antibody clone used in this study, 11G8, recognizes mouse and human ACKR3, both receptor types are visualized by ^{89}Zr-ACKR3-mAb (10,31). The capability to image human ACKR3 expression in tumors and mouse ACKR3 expression in other tissues is advantageous in allowing for a more detailed analysis of the overall ACKR3 expression profile in preclinical models compared to the use of antibodies only recognizing human or mouse receptors.

Clearance from non-specific organs such as liver and spleen was observed 120hrs post injection of ^{89}Zr-ACKR3-mAb. It should be noted that splenic venous sinusoidal endothelial cells in immunodeficient mice (6), as well as splenic marginal zone B-cells (MZB) (32), also express ACKR3 receptors, thereby contributing to the spleen uptake. In addition, low ACKR3 levels have also been reported in kidneys of immunodeficient mice, which could be a possible contributing factor for the observed renal retention (6). Accumulation of Zr-89 in bones is likely a result of ^{89}Zr-ACKR3-mAb metabolism, leading to transchelation and sequestration of Zr-89 to phosphate groups in bones. Similar bone accumulation of Zr-89 has been observed with other antibodies such as the ^{89}Zr-labeled J591 mAb, currently in clinical trials for immunoPET of the prostate-specific membrane antigen in prostate cancer patients (33,34).

CONCLUSIONS

Results from our study show that ACKR3 is highly expressed in LUSC among solid tumors. Our studies also show that ACKR3 is a viable diagnostic maker and confirm the capability of radiolabeled ACKR3-mAb for the direct, receptor-specific and non-invasive *in vivo* monitoring of ACKR3 expression with either PET or SPECT. The elasticity in the selection of imaging modality allows for chelation of a more extensive range of radioisotopes, with varying decay properties and energy windows, thus allowing for a broader array of applications. Development of ACKR3-targeted molecular imaging agents may provide a more effective route for detection of ACKR3 overexpressing cancers with currently limited diagnostic options.

Supplementary Material

Refer to Web version on PubMed Central for supplementary material.

Acknowledgments

Funding for this study was partly provided by R01CA16631 (Sridhar Nimmagadda), DoD W81XWH-12-BCRP-IDEA (Sridhar Nimmagadda) and DoD W81XWH-12-BCRP-POSTDOC2 (Babak Behnam Azad). Resources were provided by P30 CA006973 and P50 CA103175.

REFERENCES

1. Zabel BA, Wang Y, Lewen S, et al. Elucidation of CXCR7-mediated signaling events and inhibition of CXCR4-mediated tumor cell transendothelial migration by CXCR7 ligands. J Immunol. 2009; 183:3204–3211. [PubMed: 19641136]
2. Burns JM, Summers BC, Wang Y, et al. A novel chemokine receptor for SDF-1 and I-TAC involved in cell survival, cell adhesion, and tumor development. J Exp Med. 2006; 203:2201–2213. [PubMed: 16940167]
3. Luker KE, Gupta M, Steele JM, Foerster BR, Luker GD. Imaging ligand-dependent activation of CXCR7. Neoplasia. 2009; 11:1022–1035. [PubMed: 19794961]
4. Luker KE, Steele JM, Mihalko LA, Ray P, Luker GD. Constitutive and chemokine-dependent internalization and recycling of CXCR7 in breast cancer cells to degrade chemokine ligands. Oncogene. 2010; 29:4599–4610. [PubMed: 20531309]
5. Rajagopal S, Kim J, Ahn S, et al. Beta-arrestin- but not G protein-mediated signaling by the "decoy" receptor CXCR7. Proc Natl Acad Sci U S A. 2010; 107:628–632. [PubMed: 20018651]
6. Berahovich RD, Zabel BA, Lewen S, et al. Endothelial expression of CXCR7 and the regulation of systemic CXCL12 levels. Immunology. 2014; 141:111–122. [PubMed: 24116850]
7. Tachezy M, Zander H, Gebauer F, et al. CXCR7 expression in esophageal cancer. J Transl Med. 2013; 11:1–6. [PubMed: 23281771]
8. Wang J, Shiozawa Y, Wang J, et al. The role of CXCR7/RDC1 as a chemokine receptor for CXCL12/SDF-1 in prostate cancer. J Biol Chem. 2008; 283:4283–4294. [PubMed: 18057003]
9. Hattermann K, Held-Feindt J, Lucius R, et al. The chemokine receptor CXCR7 is highly expressed in human glioma cells and mediates antiapoptotic effects. Cancer Res. 2010; 70:3299–3308. [PubMed: 20388803]
10. Miao Z, Luker KE, Summers BC, et al. CXCR7 (RDC1) promotes breast and lung tumor growth in vivo and is expressed on tumor-associated vasculature. Proc Natl Acad Sci U S A. 2007; 104:15735–15740. [PubMed: 17898181]
11. Melo RCC, Longhini AL, Bigarella CL, et al. CXCR7 is highly expressed in acute lymphoblastic leukemia and potentiates CXCR4 response to CXCL12. PloS One. 2014; 9:1–12.
12. Dogan BE, Turnbull LW. Imaging of triple-negative breast cancer. Ann Oncol. 2012; 23:23–29.
13. Salazar N, Munoz D, Singh RK, Lokeshwar BL. The heterotypic interaction between CXCR7 and EGFR is an alternative proliferation mechanism in breast cancer (abstract). Cancer Res. 2014; 74:3336.
14. Wani NA, Nasser MW, Ahirwar DK, et al. C-X-C motif chemokine 12/C-X-C chemokine receptor type 7 signaling regulates breast cancer growth and metastasis by modulating the tumor microenvironment. Breast Cancer Res. 2014; 16:1–17.
15. Zhao S, Chang SL, Linderman JJ, Feng FY, Luker GD. A comprehensive analysis of CXCL12 isoforms in breast cancer. Transl Oncol. 2014; 7:429–438.
16. Ribas R, Ghazoui Z, Gao Q, et al. Identification of chemokine receptors as potential modulators of endocrine resistance in oestrogen receptor-positive breast cancers. Breast Cancer Res. 2014; 16:1–15.
17. Choi, YH., Chung, SY., Kim, JH., et al. Increase of CXCL14 and CXCR7 expression in human squamous lung cancers compared to its adjacent normal lung tissues (abstract); Paper presented at: 2015 ASCO Annual Meeting 2015; J Clin Oncol; p. e22099
18. Iwakiri S, Mino N, Takahashi T, et al. Higher expression of chemokine receptor CXCR7 is linked to early and metastatic recurrence in pathological stage I nonsmall cell lung cancer. Cancer. 2009; 115:2580–2593. [PubMed: 19309748]
19. Xu C, Fillmore CM, Koyama S, et al. Loss of Lkb1 and Pten leads to lung squamous cell carcinoma with elevated PD-L1 expression. Cancer Cell. 2014; 25:590–604. [PubMed: 24794706]
20. Wu YC, Tang SJ, Sun GH, Sun KH. CXCR7 mediates TGFbeta1-promoted EMT and tumor-initiating features in lung cancer. Oncogene. 2015:1–10.
21. Zhang XHF, Jin X, Malladi S, et al. Selection of bone metastasis seeds by mesenchymal signals in the primary tumor stroma. Cell. 2013; 154:1060–1073. [PubMed: 23993096]

22. Muller A, Homey B, Soto H, et al. Involvement of chemokine receptors in breast cancer metastasis. Nature. 2001; 410:50–56. [PubMed: 11242036]
23. Bierie B, Moses HL. Transforming growth factor beta (TGF-beta) and inflammation in cancer. Cytokine Growth Factor Rev. 2010; 21:49–59. [PubMed: 20018551]
24. Bierie B, Chung CH, Parker JS, et al. Abrogation of TGF-beta signaling enhances chemokine production and correlates with prognosis in human breast cancer. J Clin Invest. 2009; 119:1571–1582. [PubMed: 19451693]
25. Meincke M, Tiwari S, Hattermann K, Kalthoff H, Mentlein R. Near-infrared molecular imaging of tumors via chemokine receptors CXCR4 and CXCR7. Clin Exp Metastasis. 2011; 28:713–720. [PubMed: 21735100]
26. Misra P, Lebeche D, Ly H, et al. Quantitation of CXCR4 expression in myocardial infarction using 99mTc-labeled SDF-1alpha. J Nucl Med. 2008; 49:963–969. [PubMed: 18483105]
27. Berahovich RD, Penfold MET, Schall TJ. Nonspecific CXCR7 antibodies. Immunol Lett. 2010; 133:112–114. [PubMed: 20691730]
28. Lindmo T, Boven E, Cuttitta F, Fedorko J, Bunn PA. Determination of the immunoreactive fraction of radiolabeled monoclonal antibodies by linear extrapolation to binding at infinite antigen excess. J Immunol Methods. 1984; 72:77–89. [PubMed: 6086763]
29. Decaillot FM, Kazmi MA, Lin Y, Ray-Saha S, Sakmar TP, Sachdev P. CXCR7/CXCR4 heterodimer constitutively recruits beta-arrestin to enhance cell migration. J Biol Chem. 2011; 286:32188–32197. [PubMed: 21730065]
30. Busillo JM, Benovic JL. Regulation of CXCR4 signaling. Biochim Biophys Acta-Biomembranes. 2007; 1768:952–963.
31. Berahovich RD, Penfold MET, Miao Z, Walters MJ, Jaen JC, Schall TJ. Differences in CXCR7 protein expression on rat versus mouse and human splenic marginal zone B cells. Immunol Lett. 2013; 154:77–79. [PubMed: 23954811]
32. Wang H, Beaty N, Chen S, et al. The CXCR7 chemokine receptor promotes B-cell retention in the splenic marginal zone and serves as a sink for CXCL12. Blood. 2012; 119:465–468. [PubMed: 22110250]
33. Pandit-Taskar N, O'Donoghue JA, Beylergil V, et al. Zr-89-huJ591 immuno-PET imaging in patients with advanced metastatic prostate cancer. Eur J Nucl Med Mol Imaging. 2014; 41:2093–2105. [PubMed: 25143071]
34. Holland JP, Divilov V, Bander NH, Smith-Jones PM, Larson SM, Lewis JS. Zr-89-DFO-J591 for immunoPET of prostate-specific membrane antigen expression in vivo. J Nucl Med. 2010; 51:1293–1300. [PubMed: 20660376]

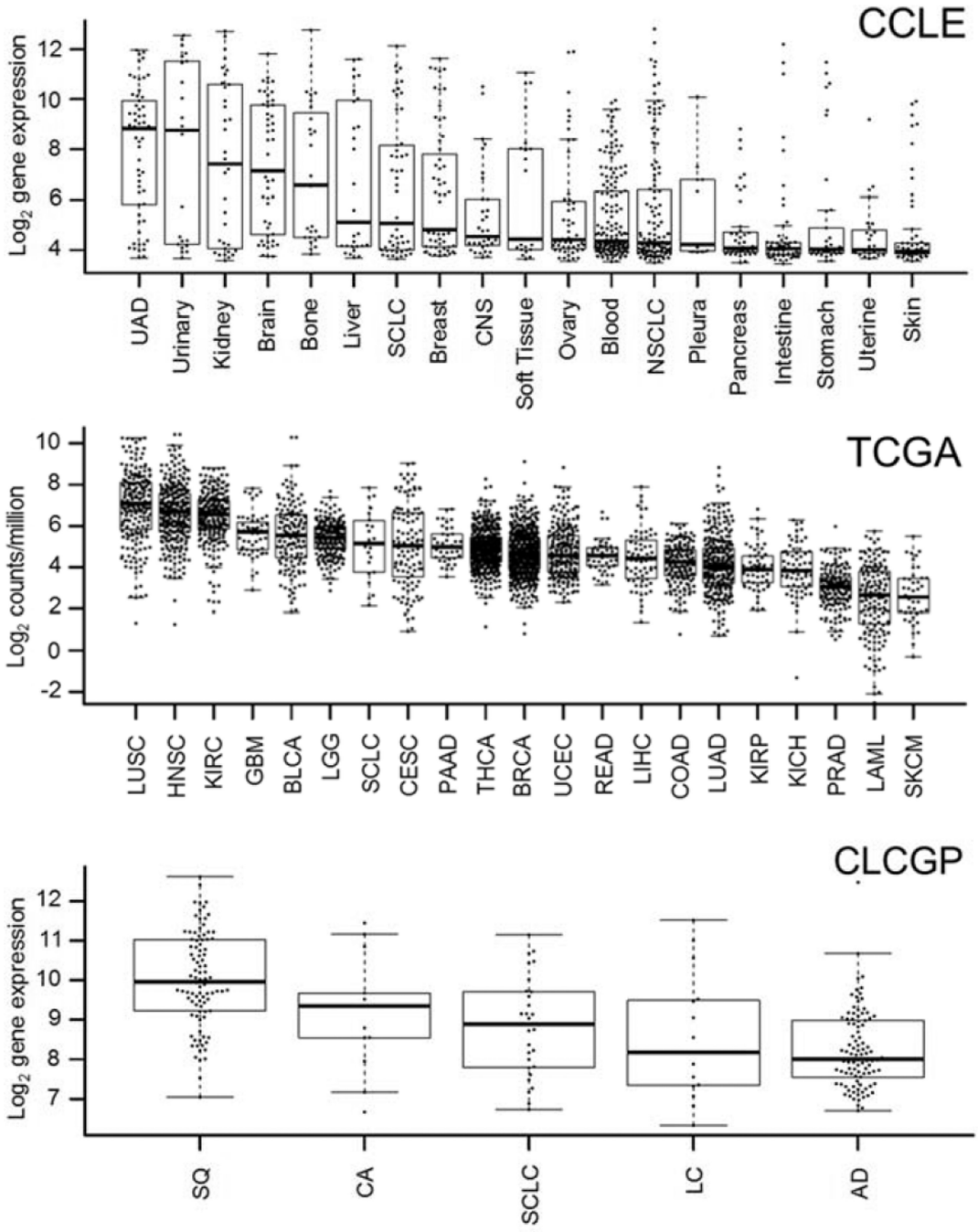

Figure 1.

ACKR3 expression in human cancers. ACKR3 mRNA expression in various cancers by CCLE and TCGA as well as CLCGP for various types of lung cancers; UAD – upper aerodigestive tract cancers, CNS – central nervous system, NSCLC – non-small cell lung cancer, SQ – squamous cell lung cancer, LC – large cell lung carcinomas, AD – lung adenocarcinomas, CA – lung carcinoid tumors, LUSC – lung squamous cell carcinoma; KIRC – kidney renal clear cell carcinoma; HNSC – head and neck squamous cell carcinoma; GBM – glioblastoma multiforme; BLCA – bladder urothelial carcinoma; LGG – brain lower

grade glioma; SCLC – small cell lung carcinoma; PAAD – pancreatic adenocarcinoma; CESC – cervical squamous cell carcinoma and endocervical adenocarcinoma; THCA – thyroid carcinoma; UCEC – uterine corpus endometrial carcinoma; BRCA – breast invasive carcinoma; READ – rectum adenocarcinoma; LUAD – lung adenocarcinoma; COAD – colon adenocarcinoma; KIRP – kidney renal papillary cell carcinoma; LIHC – liver hepatocellular carcinoma; KICH – kidney chromophobe; PRAD – prostate adenocarcinoma; LAML – acute myeloid leukemia; SKCM – skin cutaneous melanoma.

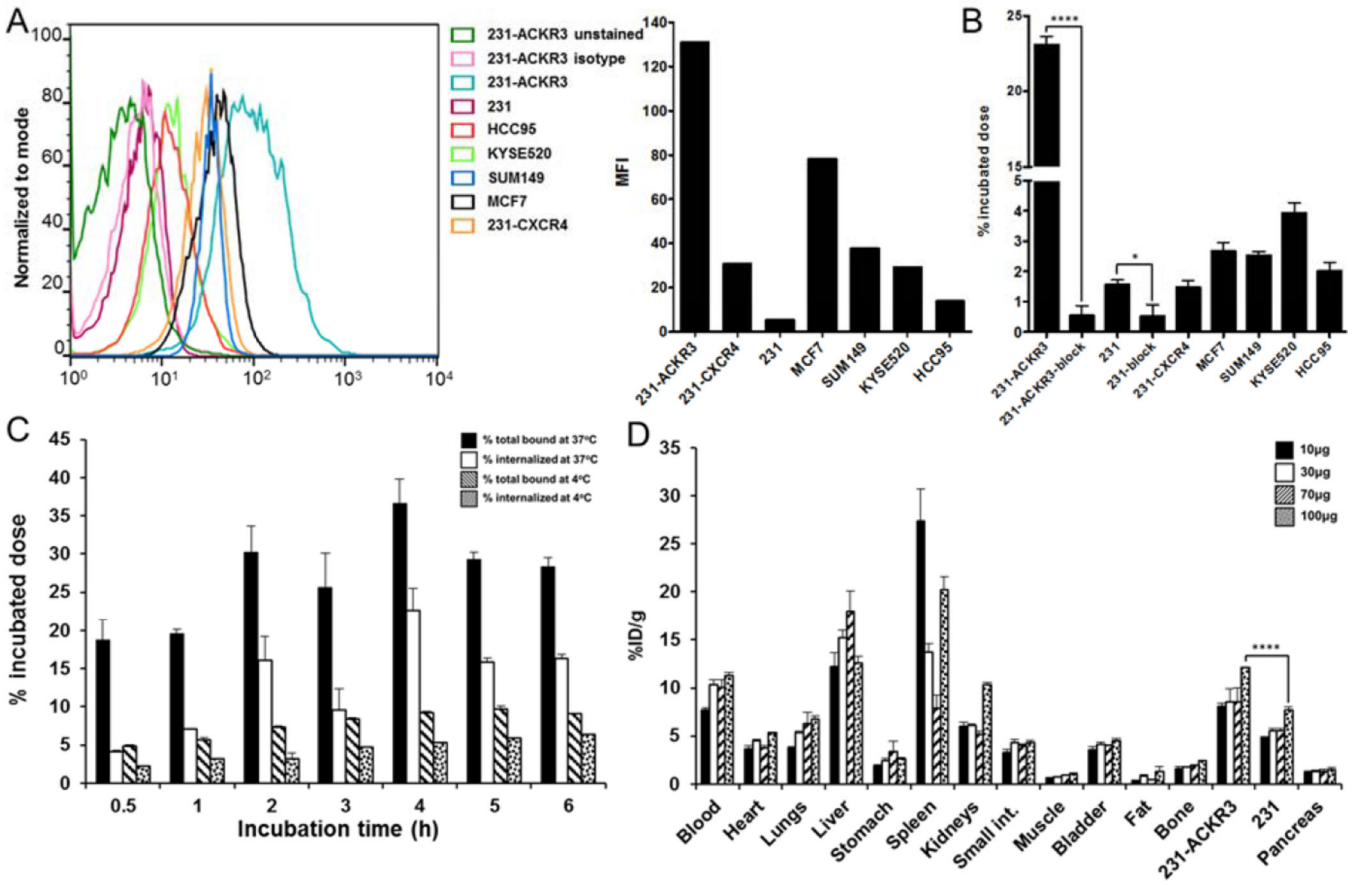

Figure 2.

Evaluation of ^{89}Zr-ACKR3-mAb *in vitro* and optimization of its specific activity *in vivo*. ACKR3 cell-surface expression by flow cytometry illustrated by overlapping histograms and mean fluorescence intensity (MFI) (A); *in vitro* binding assay with ^{89}Zr-ACKR3-mAb (B); internalization assay in 231-ACKR3 cells (C); optimization of ^{89}Zr-ACKR3-mAb specific activity using *ex vivo* biodistribution; organs from NOG mice bearing 231/231-ACKR3 tumors were harvested 48hrs post injection of 1.5MBq (40µCi) of ^{89}Zr-ACKR3-mAb accompanying 10, 30, 70 or 100µg of non-labeled ACKR3-mAb (D); 231-ACKR3 represents MDA-MB-231-ACKR3; 231 represents MDA-MB-231; 231-CXCR4 represents MDA-MB-231-CXCR4; $p \leq 0.05$ (*), ≤ 0.0001 (****).

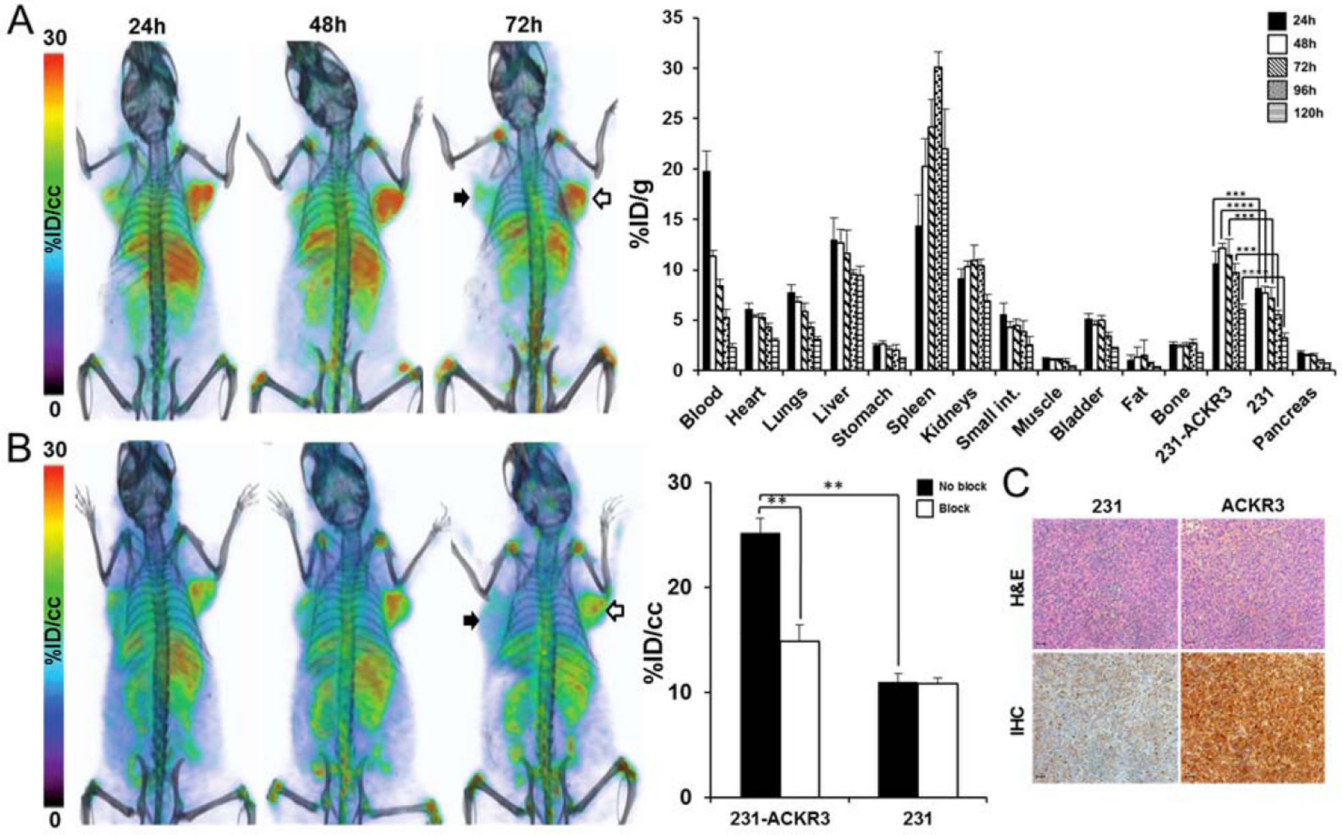

Figure 3.

^{89}Zr-ACKR3-mAb demonstrates enhanced ACKR3-mediated *in vivo* uptake by ACKR3 overexpressing TNBC. Volume rendered PET-CT imaging (left) and *ex vivo* biodistribution (right) of ^{89}Zr-ACKR3-mAb in 231 (black arrows)/231-ACKR3 (white arrows) xenografts (A); PET-CT imaging following blocking with 10meq of ACKR3-mAb (left) with *in vivo* image analysis (right) comparing blocked and non-blocked ^{89}Zr-ACKR3-mAb tumor uptake (B); H&E staining and ACKR3 immunohistochemistry of excised tumor tissues (C), scale bars represent 50μm, ACKR3 expression in IHC is demonstrated by light brown color; 231-ACKR3 represents MDA-MB-231-ACKR3; 231 represents MDA-MB-231; $p \leq 0.01$ (**), ≤ 0.001 (***), ≤ 0.0001 (****).

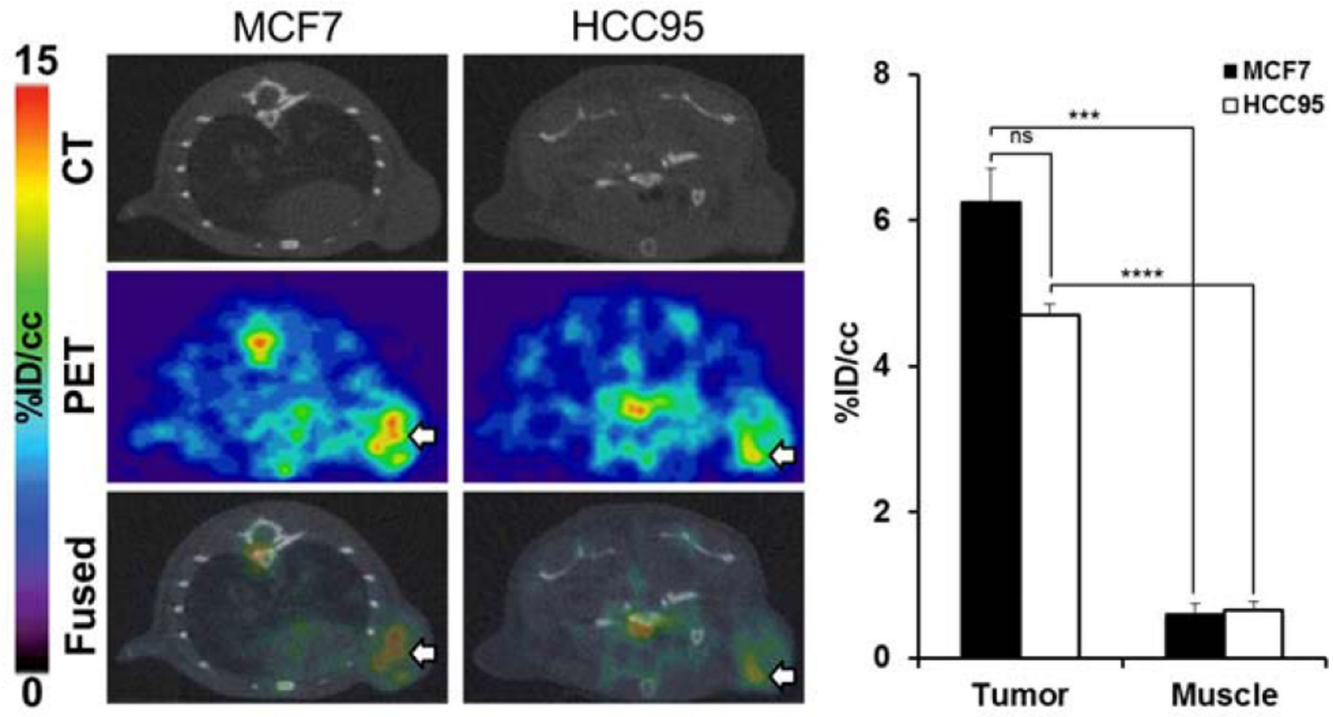

Figure 4.

^{89}Zr-ACKR3-mAb-PET detects ACKR3 overexpressing ER+ luminal A breast and LUSC tumors. Transaxial PET-CT images of MCF-7 (white arrow) and HCC95 (white arrow) xenografted mice 48hrs after a 9MBq (250μCi) intravenous injection of ^{89}Zr-ACKR3-mAb (left); quantitative PET image analysis of ^{89}Zr-ACKR3-mAb tumor uptake in MCF7 and HCC95 xenografted mice (right); $p \leq 0.001$ (***), ≤ 0.0001 (****).

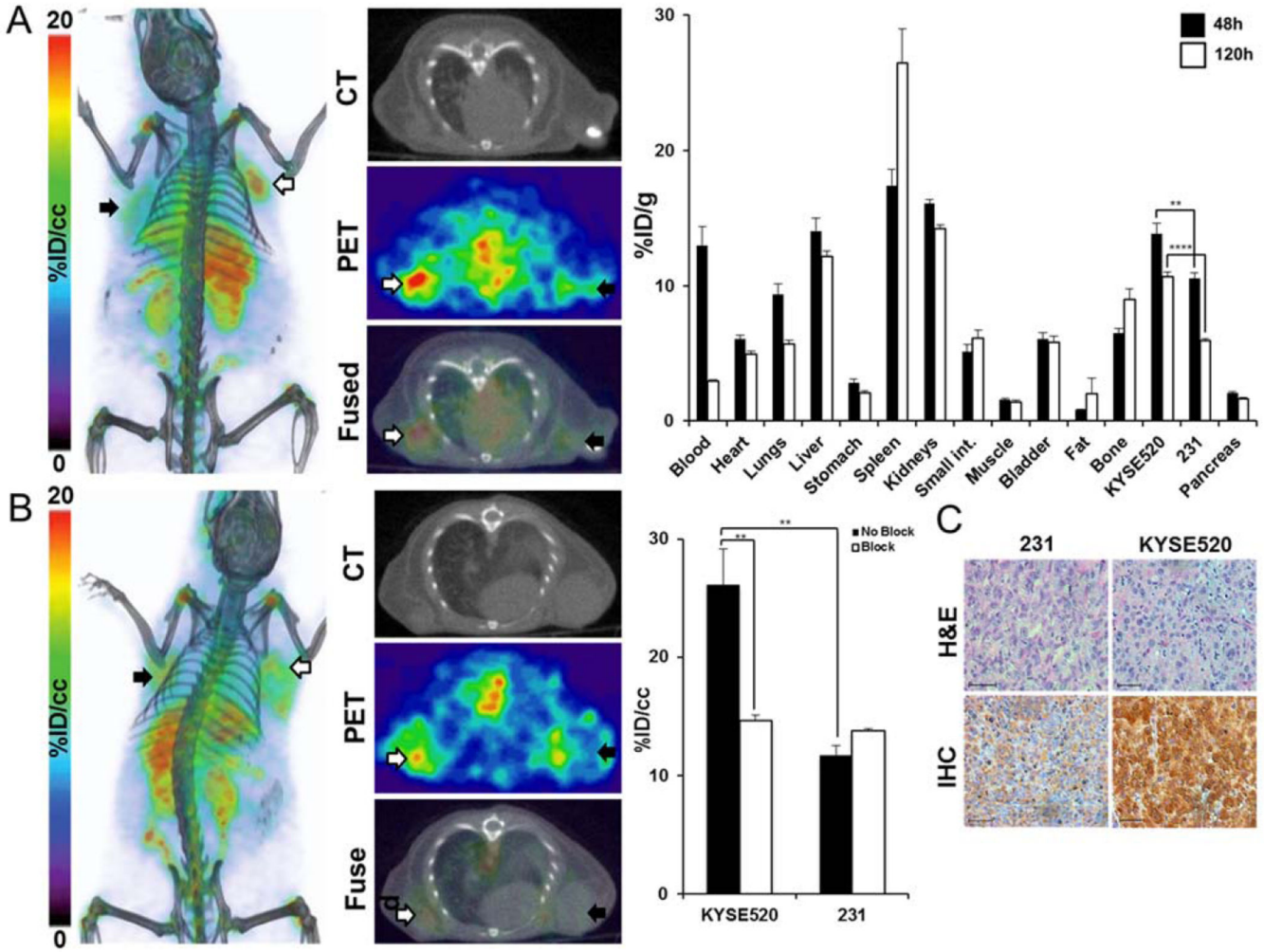

Figure 5.

^{89}Zr-ACKR3-mAb exhibits enhanced ACKR3-mediated uptake in ACKR3 overexpressing esophageal squamous small cell tumors. Volume-rendered and transaxial PET-CT images of ^{89}Zr-ACKR3-mAb 48hrs p.i. (left) as well as *ex vivo* biodistribution (right) of ^{89}Zr-ACKR3-mAb in 231/KYSE520 xenografts 48hrs and 120hrs p.i. (A); volume-rendered and transaxial PET-CT images of ^{89}Zr-ACKR3-mAb with a 10meq blocking dose of ACKR3-mAb (left) and the *in vivo* image analysis (right) comparing blocked and non-blocked ^{89}Zr-ACKR3-mAb tumor uptake (B); H&E and ACKR3 immunohistochemistry of excised 231 and KYSE520 tumor tissues (C); 231 denotes MDA-MB-231; $p \leq 0.01$ (**), ≤ 0.0001 (****).

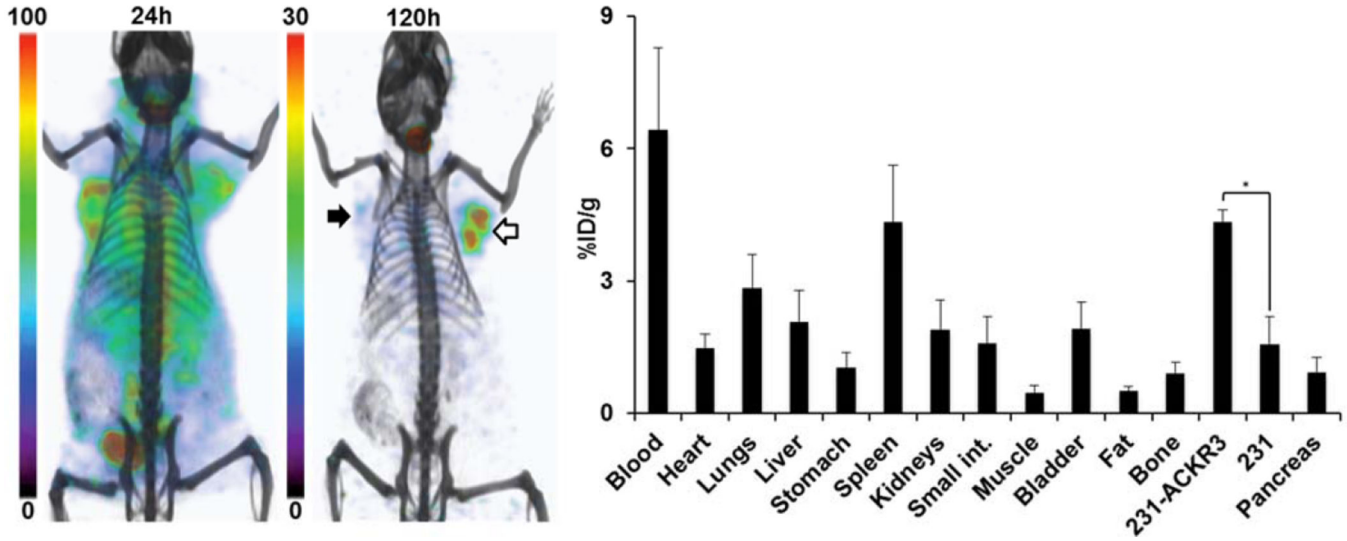

Figure 6.

Evaluation of ^{125}I-ACKR3-mAb for *in vivo* SPECT imaging of ACKR3 expression. Volume-rendered SPET-CT imaging (left) and *ex vivo* biodistribution (right) of ^{125}I-ACKR3-mAb in NOG mouse harboring 231 (black arrow) and 231-ACKR3 (white arrows) tumors, following a 37MBq (1mCi) injection of ^{125}I-ACKR3-mAb; 231-ACKR3 represents MDA-MB-231-ACKR3; 231 represents MDA-MB-231; $p \leq 0.05$ (*).